Article:
Dolan, J.F., Van Dissen, R.J., Rhodes, E.J. orcid.org/0000-0002-0361-8637 et al. (5 more authors) (2024) One tune, many tempos: faults trade off slip in time and space to accommodate relative plate motions. Earth and Planetary Science Letters, 625. 118484. ISSN 0012-821X

https://doi.org/10.1016/j.epsl.2023.118484

One tune, many tempos: Faults trade off slip in time and space to accommodate relative plate motions

J. F. Dolan[1*], Van Dissen, R. J.[2], Rhodes, E.J.[3,4], Zinke, R.[1,5], Hatem, A.[1,6]. McGuire, C.[4, 7], Langridge, R. M.[2], Grenader, J.R.[1,8]

1. Department of Earth Sciences, University of Southern California, Los Angeles, CA, USA

2. GNS Science, Lower Hutt, New Zealand

3. Department of Geography, University of Sheffield, Sheffield, UK

4. Department of Earth, Planetary and Space Sciences, UCLA, Los Angeles, CA, USA

5. Now at: NASA Jet Propulsion Laboratory, Pasadena, CA, USA

6. Now at: U.S. Geological Survey, Golden, CO, USA

7. Now at: Lawrence Livermore National Lab, Livermore, CA, USA

8. Now at: Fugro, Houston TX, USA

JFD: *Corresponding author; dolan@usc.edu
RVD: R.VanDissen@gns.cri.nz
EJR: Ed.Rhodes@sheffield.ac.uk
RZ: Robert.Zinke@jpl.nasa.gov
AH: ahatem@usgs.gov
CM: mcguire24@llnl.gov
RL: R.Langridge@gns.cri.nz
JG: jessica.grenader@gmail.com

Abstract

Analysis of incremental slip rates from the four major strike-slip faults of the Marlborough fault system (MFS) of northern South Island, New Zealand, provides a first-ever record at the scale of an entire plate-boundary fault system of how relative plate motions are accommodated in time and space. This record, which spans the past 350–450 m of relative plate motion and ca. 12–14 ky, demonstrates that the fault system as a whole accommodates a steady plate-boundary slip rate, with the MFS faults "keeping up" with the overall rate of relative Pacific-Australia plate motion at relatively short displacement (10s of meters) and time (10^2–10^3 yr) scales. These results affirm the often-assumed but until now unproven assumption that the relative plate-motion rate provides a robust basic constraint on both geodynamical models and analyses of system-level seismic hazard at these scales. In marked contrast, the incremental slip rates of each of the four main Marlborough faults are highly variable through time, marked by coordinated accelerations

and decelerations spanning 4–6 earthquakes and several millennia as the faults trade off slip to accommodate a steady relative plate motion rate. These results suggest that (a) the weakest fault in the system will slip faster than average while adjacent mechanically complementary faults slip more slowly, and (b) that these patterns switch back and forth through time, likely reflecting reversable changes in the strength (i.e., resistance to shear) of the individual faults as they collectively accommodate relative plate motion. Interestingly, the periods of fast slip on the MFS faults exhibit ~20–25 m of displacement, suggesting that these may record periods of fast slip on a weakened fault/ductile shear zone that continues until it uses up all locally stored elastic strain energy, thus potentially approaching local complete stress drop, albeit during a few tens of meters of rapid fault slip during multiple earthquakes, rather than during a single event. This hypothesis is consistent with typical earthquake stress drops of ~1-10 MPa and estimates of depth-averaged crustal shear stress of a few 10s of MPa, such as might be released in clusters of 4-6 earthquakes. These results emphasize the need to analyze the collective behavior of the entire fault systems, rather than just individual faults, to understand the mechanics of the system. Moreover, these patterns suggest a potential path forward for more accurate estimation of time-dependent seismic hazard, with the possible incorporation of current position of a fault within a fast- or slow/no-slip period into the probability analysis, as well as a means of potentially estimating crustal shear stress.

1. Introduction

Faults exhibit a wide range of behaviors, ranging from relatively regular earthquake recurrence in time and magnitude and constant slip rates (e.g., Kondo et al., 2004; Hartleb et al., 2006; Noriega et al., 2006; Kozacı et al., 2007; 2009; Pucci et al., 2007; Gold & Cowgill, 2011; Berryman et al., 2012; Salisbury et al., 2018), to highly variable displacement rates, with prolonged periods of significantly higher seismic activity and faster slip that span multiple earthquake cycles, followed by periods of relative quiescence (e.g., Wallace et al., 1987; Friedrich et al., 2003; Weldon et al., 2004; Ninis et al., 2013; Dolan et al., 2016; Zinke et al., 2017; 2019; 2021; Hatem et al., 2020). The controls on these behaviors remain poorly understood, and raise a basic question: Are variations in fault slip in time and space simply random fluctuations in a complex dynamical system (e.g., Bak & Tang, 1989; Chen et al., 2020; Gauriau et al., 2023), or are there processes that control these behaviors in systematic and potentially predictable fashion that may not yet be well understood? The answers to these questions are of fundamental importance to wide range of geoscience disciplines, from fault mechanics and geodynamics to probabilistic seismic assessment, earthquake simulations, and prediction science.

Key to addressing these questions is assessment of the behavior of entire mechanically integrated fault systems. Yet, most paleoseismic studies necessarily focus on individual faults and sites, and in general detailed, comprehensive data sets encompassing all of the major faults in a plate boundary are lacking. This knowledge gap is particularly pronounced at what we view as a critically important displacement scale of 10s to hundreds of meters that lies between single earthquake cycles typically studied with geodesy and seismology and the million-year scale constrained by global plate motion models. In this paper, we discuss our incremental slip-rate results from the main faults that comprise the

Marlborough fault system (MFS) in northern South Island, New Zealand, where Pacific-Australia relative plate motion in the crust is accommodated primarily along a system of sub-parallel dextral strike-slip and oblique reverse-dextral faults (Figure 1).

2. Observations

Over the past decade, we have used field- and lidar-based geomorphic mapping of offset stream channels (Figure 2) together with the newly developed post-IR IRSL luminescence dating technique (Rhodes, 2015) to document millennial-scale incremental slip rate records spanning the past 12–14 ka from the four fastest-slipping MFS faults – from N to S, these are the Wairau, Awatere, Clarence, and Hope faults (Zinke et al., 2017; 2019; 2021; Hatem et al., 2020). The incremental slip-rate data, collected in a roughly N-S transect approximately perpendicular to the plate motion direction and encompassing 25 separate slip rates, indicate that these four faults accommodate most, and arguably almost all, relative Pacific-Australia plate motion in the crust of northern South Island at this latitude. Specifically, adding the average latest Pleistocene-Holocene rates for all four faults yields a collective average MFS slip rate of >~31 mm/yr, indicating that these four faults accommodate at least 75-80% of the 38-40 mm/yr of relative plate motion (DeMets et al., 1994; 2010; Beavan et al., 2002; Wallace et al., 2007). This collective MFS slip rate is, however, a minimum, for two reasons. First, the three southern faults are all relatively structurally immature (i.e., each has a relatively small cumulative displacement of only ~13–20 km [Sutherland, 1999; Rattenbury et al., 2006; Zinke et al., 2015]), and thus may be characterized by significant off-fault distributed deformation surrounding the geomorphically defined fault that may remain unaccounted for and thus result in slip-rate underestimates (for example, Dolan & Haravitch, 2014 show that for faults with this cumulative displacement, fault slip measurements may commonly underestimate the total surface displacement by ~20–35%; although our measurements of large geomorphic offsets likely encompass much of this off-fault deformation, some distributed surface strain likely remains unaccounted for in our offset measurements). Second, both the Hope fault and Clarence fault slip rate sites lie near the edges of transtensional fault stepovers, which may be characterized by additional, geomorphically undetectable distributed off-fault deformation associated with these structural complexities that is not included in our dated offset measurements. This fits with the very slow (≤1 mm/yr) slip rates estimated for other faults in the MFS, although the Porter's Pass and related faults to the south of the MFS, including those that ruptured during the 2016 Mw=7.8 Kaikoura earthquake, may accommodate as much as a few mm/yr (Seebeck, Van Dissen et al. 2022). Thus, the four main MFS faults we analyzed likely accommodate almost all of the relative plate motion in the crust of this part of the plate boundary. We note that although these four strike-slip faults lie above the northwest-dipping Hikurangi plate interface, the plate interface megathrust fault lies at or below the northwest-deepening, 35- to 50-km-deep Moho beneath our four study sites at depths ranging from ~35 km beneath the Hope fault study site to ~45 km beneath the Clarence and Awatere fault sites to ~65 km beneath the Wairau fault study site (Eberhart-Phillips & Bannister 2010; Eberhart-Phillips et al., 2010; 2014; Williams et al. 2013).

The incremental slip rate records of the four main MFS faults are summarized in figures 3, 4, and 5 and Table 1. These results provide the most detailed incremental rate record for all the major faults in a plate-boundary fault system yet generated, and allow us, for the first time, to "dissect" the distribution of relative plate motion displacements amongst the major faults that comprise the plate boundary system, providing key constraints on how plate boundary slip is accommodated in time and space. Several key results are observable in this compilation.

Most basically, these data demonstrate that over the past 350–450 meters of relative Pacific-Australia plate motion, the overall rate has been relatively constant throughout the c. 12–14 ky period of our analysis. In marked contrast to the near-constant total system-level relative rate, the incremental slip rates of the individual faults have varied considerably, by as much as a factor of 7x for the Awatere fault, for example, over displacement increments of several 10s of meters (Zinke et al., 2017). The Wairau and Clarence faults exhibit similar extreme variations in incremental slip rate spanning multiple earthquake cycles (Zinke et al., 2019; 2021). Variations in slip rate along the faster-slipping Hope fault appear more subdued, but as Hatem et al., 2020 noted, this is likely a function of the fact that the slip-rate increments on that fault generally span large displacements and numerous earthquakes (e.g., the three oldest Hope fault incremental slip rates span 48 to 71.5 m, relative to most of the 21 other incremental rates, which span ≤26 m of slip), averaging over any smaller-displacement/shorter-term accelerations and decelerations in fault slip that have occurred, whereas the records from the three slower-slipping northern faults approach earthquake-by-earthquake level detail over much of the past 12–14 ka (Zinke et al., 2017; 2019; 2021). Our statistical analyses demonstrating the variability of the incremental slip rate records of each of the MFS faults, and the relative constancy of the ensemble, system-level rate are summarized in figure 5 and Table 1, and described in detail in S1 and S2).

Interestingly, the slip-rate variations on these faults do not appear to be random. Rather, the data reveal patterns of apparently coordinated waxing and waning of incremental slip rate amongst the four faults. For example, both the Wairau and the Clarence faults exhibited much faster-than-average slip rates during latest Pleistocene-early Holocene time (ca. 8–12 ka), bracketed by periods in which they slipped much more slowly, whereas the Awatere fault between them exhibited the opposite pattern, with a relatively slow slip rate during the earlier part of the record, and accelerated slip rate during mid- to late-Holocene time since ca. 8 ka (Figures 3-5; Table 1; S1).

When viewed as a sub-system within the MFS, as shown by the umber curve in figure 4B, the collective slip rate of the northern three faults was relatively fast during the first half of the record prior to ca. 5 ka and slowed during mid-Holocene to recent time. The slip rate of the Hope fault, with an average rate of 15-20 mm/yr, sub-equal to the collective rate of the three northern MFS faults and 3–4X faster than the individual slip rates of the three northern faults, has exhibited the opposite pattern, with relatively slow slip at ~13 mm/yr year during latest Pleistocene-mid Holocene time and much faster average slip at ~19 mm/yr encompassing the past 100 m of fault slip since ca. 5.4 ka (Hatem et al., 2021).

Another noteworthy observation is that the amount of displacement that occurred in each of the "fast" periods (noted on figure 5) on the MFS faults appears to be similar. Specifically, of the six fast intervals we documented along these four faults, four of them resulted from 20–25 m of total displacement (Wairau fault [2.0-4.3 ka and 8.6-10.1 ka]; Awatere fault [4.3-5.2 ka]; Clarence fault [9.0-11.2 ka]; Zinke et al., 2017; 2019; 2021), a fifth was ≥17.5 m (Hatem et al., 2020), and the sixth was at least 11 m, and we suspect 23 m (Awatere fault [7.6-8.1 ka, and possibly 5.2-8.1 ka]), although we lack the resolution to constrain incremental offsets versus earthquake ages over this time interval at that site (Zinke et al., 2017). Thus, all of these fast intervals seem to have encompassed ~20–25 m of slip that occurred during multiple surface ruptures, with these fast intervals separated by millennia-long lulls involving either no or slow fault slip (Figures 3, 4, and 5; Table 1).

3. Discussion

What can these data tell us about how plate boundaries accommodate relative motion on faults in the crust? Most basically, the constant overall system rate suggests that the faults are responding to a simple steady-state boundary condition imposed by the relative plate rate. Moreover, the relative steadiness of the system-wide rate indicates that the fault system, when viewed as a mechanically integrated whole, "keeps up" with the rate imposed by the relative plate rate boundary condition at brief (≤millennial) time scales and small relative plate motion displacement scales (≤a few 10s of meters).

In addition, the basic constraint supplied by the relatively constant system rate, coupled with the highly variable incremental rates of the individual constituent faults, leads to the twin realizations that (a) the variable slip rates on the individual faults that comprise the MFS are driven by processes intrinsic to the system, that is, that originate within the fault system, and (b) that whatever these mechanisms are, they operate at displacement scales that are much larger than those of individual earthquakes, and they must toggle back and forth for individual faults over millennial time scales and a few tens of meters of fault slip, as shown by the complementary waxing and waning of slip rates on the MFS faults.

These observations suggest that when there are mechanically complementary faults in an integrated mechanical system such as the MFS, the faults operate in a delicate balance in which whichever of the faults is less resistant to shear (i.e., "weaker"), the faster that fault will slip and the more of the overall system-level rate it will accommodate during that period. Conversely, if a mechanically complementary fault in the system is even slightly more resistant to shear, it will exhibit a slower slip rate and do less of the overall work accommodated by the system during that period. This model implies that the MFS faults are "communicating" across the scale of the entire fault system, likely through some combination of stress interactions in the brittle upper crust and/or viscoelastic processes associated with shear along the deep ductile roots of the faults, such that at least one fault in the system is slipping over short time and displacement scales as the system responds to the basic boundary condition imposed by the relative plate motion rate.

Perhaps the most curious aspect of this fast-slow incremental slip rate behavior is the occurrence of the fast periods. Why would one fault continue to slip much faster than its

average rate for tens of meters of slip spanning multiple earthquakes when there are other, mechanically complementary faults nearby that can accomplish the same work? This behavior is especially interesting when thought of in terms of stress evolution of the fault. Specifically, when a fault slips, it redistributes the stress acting on it, leaving a "stress shadow" that moves the fault farther away from failure, with the shadow deepest along the rupture plane itself (e.g., Harris & Simpson, 1996; 1998; Harris, 1998). Yet, the incremental fault slip rates we document for the four main MFS faults demonstrate that each of these faults has experienced periods of significantly faster-than-average slip that span multiple earthquake cycles and 10s of meters of fault displacement. If failure stress on the fault is reduced every time it slips, then how and why could this be so? These observations require some mechanism(s) that cause the fault to keep slipping faster than average over multiple earthquake cycles, and place significant constraints on what mechanisms may be controlling this behavior.

What mechanisms might control such alternating fast and slow periods of slip on individual faults? We suggest that this behavior likely reflects changes in the strength of the faults (i.e., their resistance to shear) back and forth through time, such that if a fault that had been slipping fast strengthens, the other faults in the system become the relatively weaker elements and begin slipping faster to maintain the constant system-level rate (Figure 5). For example, Dolan et al. (2007) suggested that the ductile roots of the fault might gradually strain harden following an extended period of anomalously rapid fault slip, reducing the loading rate of the upper crustal, seismogenic fault. This might be particularly effective within and just below the brittle-ductile transition, a depth range characterized by both low temperatures and high stresses where dislocation glide mechanisms and associated strain hardening may be dominant over other crystal plastic deformation mechanisms that operate at higher temperatures at deeper depths (Ashby & Verrall, 1978 [their "low-temperature plasticity"]). Following a period of fast ductile slip, the ductile roots of the fault would then slip more slowly or not at all, and anneal during the subsequent lull in slip, gradually weakening and preparing the fault for the next "fast" period. During the subsequent fast period, the weakened ductile shear zone roots will shear more rapidly, loading the upper crustal seismogenic part of the fault faster than average, resulting in more frequent and/or larger earthquakes. In a potential feedback loop, the resulting earthquake clusters on upper crustal fault would increase shear stresses on their ductile shear zone roots, increasing ductile shear zone shearing rates. Such changes might be manifest in geodetic data, but may be difficult to detect (e.g., Dolan & Meade 2017).

An alternative and potentially complementary possibility is that fluids, either through their addition or removal, could modulate the strength of ductile shear-zone roots. In particular, it has been suggested that the addition of fluids will weaken the ductile shear zone, leading to faster shearing rates that load the upper crustal fault above. For example, Oskin et al. (2008) suggested that fluids might be expelled downward into the underlying ductile shear zone in response to stress changes following a large earthquake on the brittle fault in the upper crust, causing the ductile shear zone to weaken and slip faster. But Dolan et al., (2016) noted that pressure gradients are likely to almost always be upwards within fault zones, making this possibility unlikely. Moreover, Bürgmann and Dresen (2008) noted that that almost all ductile shear zones at these crustal levels contain some crystalline water,

and Kronenberg et al. (2020) suggest that it is the presence of water, rather than the amount of water, that strongly modulates the strength of ductile shear within and just below the brittle-ductile transition. Alternatively, it is possible that dehydration of the ductile shear zone (e.g., Finch et al., 2016) alternating with re-hydration of the shear zone in response to the chemical potential gradient established between a dry inner shear zone and hydrous wall rocks may modulate the resistance to shear and the resulting slip rate of ductile shear zones (Dolan & Meade, 2017).

The observation that the fast periods on all strike-slip faults we have studied thus far have a finite, and similar, amount of displacement suggests the potentially complementary possibility that individual faults, once weakened, may slip faster for a finite total displacement as they "use up" all, or almost all of the elastic strain energy resolved on that fault (i.e., the fault may approach complete stress drop, although over a span of multiple earthquakes and tens of meters of fault slip, rather than during a single event). It has long been suggested that the crust stores significantly more elastic strain energy than is released in a single earthquake. For example, following on paleoseismic observations of an extremely rapid period of slip spanning ≥~20 m of displacement in five earthquakes between ca. 600–850 CE on the San Andreas fault at Wrightwood (Weldon et al., 2004), Fay & Humphreys (2006) compared stresses derived from a force and torque balance in the Salton block in southernmost California to estimate that there may be enough "excess" stored elastic strain energy to drive at least 4–5 large-magnitude earthquakes, assuming a typical stress drop in each earthquake of 1-10 MPa. Similarly, Fialko et al. (2004) used along-strike variations in topography along the San Andreas fault and the geometry of the fault to infer fault-averaged shear stresses of the order of 20–30 MPa. More recently, Fialko (2021) used relative attitudes of conjugate faults that ruptured during the 2019 Ridgecrest, California, earthquake sequence to estimate a similar depth-averaged shear stress in the crust of 25–40 MPa. All of these studies suggest that depth-averaged shear stresses on major faults in California are on the order of a few tens of MPa, similar to the cumulative stress drops that would be observed from 4–6 earthquakes. We refer to this excess elastic strain energy stored in the crust as the crustal strain capacitor, since it can be drawn upon to drive additional earthquakes. Interestingly, as noted above the amount of slip during fast periods of slip on the three northern MFS faults all equal ~20–25 m (Zinke et al., 2017; 2019; 2021), as does the youngest such fast period documented on the Hope fault (Hatem et al., 2021). In two of the only other sufficiently detailed available incremental slip-rate records, the Garlock fault experienced ~26 m of slip in a cluster of 4–5 large-magnitude earthquakes between 0.5–2.0 ka (Dawson et al., 2003; Dolan et al., 2016; Peña et al., 2018) similar to the ≥~20 m of slip in the 600–850 CE fast period along the San Andres fault at Wrightwood (Weldon et al., 2004). Although robust assessment of this possibility remains data-limited, the overall similarity of these values suggests that slip of ~20–25 m may represent the maximum amount of resolved elastic strain energy that is "stored" on each fault (or at least whatever shear strain energy can be effectively released through fault slip above some semi-permanent threshold value). We suggest the possibility that once whatever weakening mechanism(s) that control the initiation and maintenance of a period of fast slip take over that the fault will continue to slip, drawing on the crustal strain capacitance until the fault simply runs of out "fuel" (i.e., shear stress/resolved elastic strain energy), at which point the fault slip will switch to the next-weakest fault in the

mechanically integrated network of complementary faults in order to maintain the overall constant plate rate.

If other faults elsewhere can be shown to exhibit this same range of displacements during periods of fast slip, this may (a) allow estimates of absolute level of elastic strain energy (stress) stored in the crust; and (b) hold out the promise of better forecasting the likelihood of near-future earthquakes on a specific fault if the incremental slip rate record is known. For example, if a fault is shown to have experienced a recent large earthquake following a long period of slow or no slip whose duration spans multiple average earthquake recurrence intervals, then the fault may be entering a period of fast slip. Conversely, if a fault is shown to have experienced a period of faster-than-average displacement spanning several earthquakes and totaling on the order of 20-25 m of displacement, then the fault may have exhausted its crustal strain capacitor and may be entering a quieter mode. For example, the Wairau fault, which has a near earthquake-by-earthquake incremental slip-rate record spanning the past 12 ky (Nicol & Van Dissen, 2018; Zinke et al., 2021), slipped ~25 m during five earthquakes between 2 ka and 5.4 ka, after which the fault has been quiescent. If we had paleoseismic data showing that the fault had just gone through a period of accelerated slip spanning 25 m of displacement (i.e., if we were doing this analysis 2,000 years ago), we might have been able to suggest that the likelihood of a near-future earthquake on the Wairau was relatively low, allowing more accurate probabilistic estimates of earthquake occurrence on this fault. More-refined incremental slip-rate records from more faults in more plate boundary fault systems are necessary to evaluate this possibility, but if such records do become available in the future, this may provide a path forward to better estimation of the probability of near-future earthquakes as the position within a "fast period" could be evaluated in a quantitative sense. Moreover, periods of faster ductile shear-zone slip and commensurately faster loading of the upper crustal, seismogenic parts of the fault, may be observable geodetically, leading to higher estimates of the probability of a near-future earthquake. Conversely, slower-than-average ductile shear-zone rates manifest as slower geodetic rates might be used to suggest a lower probability of near-future seismic slip (e.g., the current relatively slow geodetic rate on the Mojave section of the San Andreas fault; Dolan et al., 2016; Evans et al., 2018).

4. Conclusions and Implications

Comparison of incremental slip-rate records from the four major strike-slip faults that comprise the Pacific-Australia plate boundary in northern South Island, New Zealand, reveals that, although the slip rates of individual faults vary widely through time, with fast periods accommodating 20–25 m of slip during sequences of 4–6 earthquakes separated by lulls of slow or no slip, the overall, system-level rate is constant. These results have basic implications not only for our understanding of how plate-boundary fault systems work to collectively accommodate relative motions, but also for attempts to understand and potentially forecast the probability of occurrence of major earthquakes. What can these data tell us about the predictability of the behavior of such fault systems? At the scale of individual earthquakes, in complex plate-boundary fault systems like the MFS that are composed of multiple, mechanically complementary faults in which irregular incremental slip rates may be the norm (Gauriau & Dolan, 2021), the occurrence of any individual

earthquake may be random, controlled by a myriad of poorly understood (and potentially unmeasurable) factors (e.g., previous stress history related to both the previous earthquakes on the fault and other faults in system, but also by spatially variable displacement in earlier ruptures, potentially transitory fluid pressures, contact friction evolution, and temporally variable mechanical properties of fault-zone rocks). Indeed, attempts to use simple physical models of earthquake recurrence on individual faults (e.g., time- and slip-predictable behavior; Bufe et al., 1977; Shimazaki & Nakata, 1980) in such multi-fault plate-boundary fault systems have usually failed (e.g., as demonstrated by Weldon et al., 2004, for the San Andreas fault at Wrightwood), indicating that much more complex controls are at work, rather than the steady loading rates and invariant fault-zone strength envisioned in these simple models. Even the longest paleoseismologic record of individual earthquakes in the world (the Hokuri Creek site on the Alpine fault; Berryman et al., 2012), which exhibits a very low COV of 0.3 and quasi-periodic earthquake recurrence, may best be characterized as the result of a fundamentally chaotic underlying mechanical system (Gauriau et al., 2023 in press).

It is only by looking beyond the single-earthquake cycle and single-fault scales at the behavior of the entire fault system over multiple-earthquake time and displacement scales that sense can be made of these behaviors. Specifically, the incremental slip-rate records from the four main MFS faults demonstrate that, while slip on the individual faults is highly irregular through time, the cumulative system-level rate is nearly constant at the 12-13 ky time scales and 350-450 m of relative plate motion that we document, demonstrating that the relative plate motion rate (and by extension system-level seismic moment accrual rates) is maintained at a relatively constant rate at both small system-level displacement scales (a few 10s of meters) and brief timescales (≤a few centuries). These data thus provide a robust boundary condition with strong predictive value and affirm the often-assumed, but until now unproven at these displacement scales, assumption that the relative plate-motion rate provides a robust basic constraint on both geodynamical models and analyses of system-level seismic hazard, as in physics-based earthquake simulators and regional probabilistic seismic hazard analyses (e.g., Field et al., 2015; 2017).

Moreover, the MFS incremental slip-rate records, together with other similar records from other major plate boundary-scale strike-slip faults, provide tight constraints over the displacement (~20-25 m) and time (centennial-millennial) scales at which whatever mechanical processes control these behaviors operate. In addition to helping to constrain possible candidate mechanisms (e.g., strengthening of fault-zone rocks within either the upper seismogenic or lower ductile crust, introduction or removal of fluids and ductile shear-zone response), these observations hold the promise of being potentially useful in both probabilistic seismic hazard assessment and operational earthquake forecasting (e.g., Jordan et al., 2014; Field et al., 2016; Field, 2019), as well as estimation of absolute stress levels in the crust.

Taken together, these data support a model of mechanically integrated faults working collectively to accommodate plate-boundary motion, with the weakest fault in the system (and/or the fault with the highest stored elastic strain energy) accommodating faster-than-average slip for a finite period/displacement while other faults in the system slip more

slowly or not at all. Maintaining the observed constant system-level rate requires that the system communicates the fact that one fault is slipping faster than average across the entire system such that other faults are not required to slip as fast. The brief time (≤a few centuries) and displacement (≤a few 10s of m) scales over which the plate boundary maintains a constant rate suggest that the system cannot store much shear strain energy before some component of the mechanically integrated system will slip. This suggests that the "strength" of the entire system may be ultimately controlled by whichever is the weakest fault in the system at any particular time, and this will change with time as the faults that comprise the system speed up and slow down in concert in response to a steady plate-rate boundary condition.

Acknowledgments

This research was funded by U.S. National Science Foundation grants EAR-1321914 (Dolan) and EAR-1321912 (Rhodes) and by GNS Science. We have benefitted greatly from fruitful discussions with Sylvain Barbot and Judith Gauriau regarding these results. Thanks to two anonymous reviewers for their constructive comments. Finally, we would like to thank all of the landowners who granted us access to their properties to conduct this research.

Figure Captions

Figure 1 Map of active tectonics of New Zealand showing faults of the Marlborough fault system, (MFS) and our four study sites. Inset shows tectonic setting of New Zealand. Black lines show dominant faults proximal to the study area (Litchfield et al., 2014). Main figure shows the location of our study sites along the four fastest-slipping MFS faults (bold black lines): (BR) and (DB) are the adjacent Branch River and Dunbeath sites on the Wairau fault (Zinke et al., 2021); (SR) Saxton River site on the Awatere fault (Zinke et al., 2017); (TR) Tophouse Road/Clarence River site on the Clarence fault (Zinke et al., 2019); (HS) Hossack Station on the Hope fault (Hatem et al., 2020). Thin black lines represent slower-slipping structures. Gray arrow shows the relative Pacific-Australian plate motion vector at 38-40 mm/yr (DeMets et al., 1990; 1994; 2010; Beavan et al., 2002; Wallace et al., 2007).

Figure 2 Oblique aerial photo looking eastward down Wairau Valley across Branch River, a major north-flowing tributary that drains into the eastward-flowing Wairau River out of view to the left (North) of the field of view, illustrating fault offsets typical of our study sites. The Wairau fault (marked by orange arrows) offsets six prominent fluvial terrace risers that mark progressive downcutting of the Branch River floodplain, denoted by short lines marking the positions of offset terrace risers (Lensen, 1968; Zinke et al. 2021). Progressive downcutting of Branch River has resulted in progressively younger and lower terrace riser offsets down to the currently active Branch River floodplain in the foreground. The youngest offset (yellow lines) of 26.5 +1.5/-0.8 m at this site is dated at 8.6 ± 0.5 kyb 2018 (thousands of years before 2018 CE), whereas the oldest offset of 58 ± 3 m (green lines) is dated at 11.9 +1.0/-0.8 kyb2018 by Zinke et al. (2021). The six dated offsets at the Branch River site provide part of the incremental slip-rate record of the Wairau fault

documented by Zinke et al. (2021) and illustrate the approach used in determining the incremental slip-rate records of all four of the main dextral strike-slip faults that accommodate Pacific-Australia relative plate motion in the Marlborough Fault System. Note that not all offset features at this site are shown (e.g., prominent offset fluvial channels between pink and pale orange lines). Lloyd Homer photo #5051 used with kind permission from GNS Science.

Figure 3 Incremental fault slip-rate data from the four main Marlborough fault system faults discussed in this paper. The study sites on these four main faults – from north to south the Wairau, Awatere, Clarence, and Hope faults – are shown atop a map of active faults in this portion of the Pacific-Australia plate boundary. See Zinke et al. (2017; 2019; 2021), and Hatem et al., (2020) for detailed descriptions. The four MFS faults are labelled, as well as represented by different colors (Wairau=red; Awatere=green; Clarence=brown; Hope=purple). BR+DB is Branch River-Dunbeath site of Zinke et al. (2021); SR is Saxton River site of Zinke et al. (2017); TR is Tophouse Road site of Zinke et al. (2019); HS is Hossack Station site of Hatem et al. (2020). Note that incremental slip rate records – that is, records that comprise multiple separate slip rates spanning different increments of displacement on a single fault at the same location – differ from what we might term "traditional" fault slip rates, which are typically based on the average rate since initiation of offset of a single dated offset.

Figure 4 Summary of incremental fault slip rate data for the Marlborough fault system plotted as cumulative displacement on vertical axis and time from the present back to 15 thousand years ago (ka) on the horizontal axis. (A) Individual incremental slip rates for the four MFS faults (Wairau=red; Awatere=green; Clarence=brown; Hope=purple) as well as the cumulative slip rate across the entire system (black lines). Each of these records shows the results of a million Monte Carlo runs using the RISeR program (Zinke et al., 2021; https://github.com/rzinke/RISeR; https://doi.org/10.5281/zenodo.4733235) through the error limits of each of the incremental slip-rate records as well as the cumulative record. Note the tradeoff amongst the highly irregular incremental slip rates for each fault but the constant overall system-level rate (see S1 and S2 for discussion of our statistical documentation of the variability in incremental slip rate on individual faults and the relative constancy of the ensemble, system-level rate) . Dashed lines show reference rates in 5 mm/yr increments at 25 mm/yr through 40 mm/yr. (B) Expanded view of the trade-off in slip through time for the northern three faults (same colors as in [a] but note change in range of displacements shown on vertical axis) as well as their cumulative rate (umber lines) compared with the incremental slip rate of the Hope fault (purple).

Figure 5 Probability density functions (pdfs) of the 25 incremental slip rates determined for the four Marlborough faults, compiled from data in Zinke et al., 2017; 2019; 2021) and Hatem et al. (2020), and shown in numerical form in Table 1. Each pdf shows the results of 1,000,000 Monte Carlo runs through the entire error limits of each measurement using the RISeR program (Zinke et al., 2021). The darker part of each pdf shows the 68% confidence limits, whereas the paler colors show the full 96.4% (2 sigma) confidence limits, for each incremental slip rate. The horizontal axis shows slip rate in mm/yr, increasing to the right. Note that the vertical axes of these plots do not denote linear time,

but rather the age ranges over which each of the incremental rates is averaged, with the oldest increment at bottom. Each incremental rate is described at left, beginning with the time interval over which that incremental rate is determined in ka, followed in parentheses by the duration of that increment in ky (kilo-years); the displacement interval over which that incremental slip rate is documented in meters, followed in parentheses by the total displacement during that increment in meters; and finally the slip rate determined over that interval in mm/yr. Note periods of faster than average slip rate spanning 20-25 m of displacement (highlighted in red font) from 2.0 to 4.3 ka and $8.6^{\pm 0.5}$ to 10.1 ka on the Wairau fault (the slow-/no-slip interval from 9.0-9.6 ka likely records the time between successive earthquakes during the period of fast slip) that are separated by a 3.4 ky-long interval of no slip from 4.3 to 8.6 ka (Zinke et al., 2021). On the Awatere fault, a period of relatively slow slip since 4.3 ka was preceded by a period of very fast slip spanning 20.5 m displacement between 4.2-5.2 ka, and another fast period spanning at least 11 m, and likely 23 m, of displacement that began at 8.1 ka and ended sometime before 5.2 ka (Zinke et al., 2017). The Clarence fault has been slipping relatively slowly since early Holocene time (9.0 ka), but the current slow rate was preceded by a period of exceptionally fast slip spanning 25.5 m of displacement from 9.0-11.2 ka (Zinke et al., 2019). The slip rate of the Hope fault is much faster than the other three main MFS faults, and consequently the three oldest slip-rate increments span larger displacement intervals (71.5 m, 48 m, and 61 m) than any of our other 22 incremental slip rates. In contrast to the apparent relative constancy of rate from this older part of the Hope fault record, the more tightly constrained, youngest part of the record reveals pronounced variations in incremental slip rate similar to the other three faults, with the 8.2 mm/yr rate since 1.4 ka preceded by a rate of 33 mm/yr from 1.4 to 1.6 ka (Hatem et al., 2020).

Figure 6 Schematic diagram showing our hypothesized evolution of the controls on the behavior of the system of four main fault that comprise the Marlborough Fault System discussed in this paper. Illustrated on the figure are the changing relationships amongst incremental fault slip rates and hypothesized fault strength and crustal shear stress changes through time on two idealized, mechanically complementary, parallel dextral strike-slip faults (Faults 1 and 2) that trade off slip to maintain an overall constant system-level rate of shear. Figures 5A through 5D represent snapshots of these co-varying parameters at different stages in the evolution of this system from fault 1 being the active fault in the system, to slip on that fault waning as a fast period of slip begins on Fault 2. BDT = Brittle-Ductile Transition zone, with an approximate depth extent shown for generic continental crust. (5A) Figure 5A shows the beginning of the idealized trade-off cycle, with fault 1 slipping much faster than its long-term average rate in a series of large earthquakes. In this phase, we hypothesize that fault 1 is the weakest fault in the system (i.e., that its resistance to shear, either in the ductile shear zone roots and/or the upper, seismogenic part of the fault, is lower than other mechanically complementary faults in the system). This fast slip is facilitated by storage of several 10s of MPa of shear stress in the crust around the fault, combined with a low resistance to shear to drive Fault 1 much faster than its average rate during this period. During this phase, while Fault 1 is slipping fast, parallel Fault 2 is slipping either slowly or not at all since the system-level load is being accommodated primarily by Fault 1. (5B) During this period, Fault 1 continues to slip fast as a result of continued fault weakness, but the driving shear stress in the “crustal strain capacitor”

surrounding Fault 1 is starting to become depleted. Meanwhile, the crustal strain capacitance around Fault 2, which was assumed to be depleted at the beginning of this sequence in figure 5A, is gradually increasing, as is the weakness of Fault 2, perhaps through annealing of strain-hardened shear zone rocks resulting from the previous phase of rapid Fault 2 slip (prior to time step shown in figure 5A). (5C) Figure 5C shows a period in which the crustal strain capacitor surrounding Fault 1 has been depleted in a cluster of large-displacement earthquakes that cumulatively resulted in displacement along Fault 1 of ~20-25 m. Moreover, during the waning stages of the Fault 1 fast period, Fault 1 has likely also become mechanically stronger. The combination of lowered driving stress and a mechanically stronger fault that is more resistant to shear results in cessation of slip on Fault 1. Simultaneously, Fault 2, which has gradually weakened through stages 5A and 5B, reaches a point where it has become weaker than Fault 1. In addition, during the preceding periods shown in 5A and 5B, the crustal strain capacitance in the crust surrounding Fault 2 has increased, although not necessarily at a constant rate (i.e., the ductile roots of Fault 2 may have been more resistant to shear during the preceding period of slow or no Fault 2 slip, resulting in slower loading of the Fault 2 crustal strain capacitor). These changes favor Fault 2 becoming the dominant fault in the system during the next stage. (5D) The crustal strain capacitor surrounding fault 2 has been filled, and together with potential weakening of Fault 2 during its preceding period of slow or no slip (stages 5A through 5C), Fault 2 begins to slip fast in a series of large earthquakes, completing the trade-off of active slip from Fault 1 shown in figures 5A and 5B to Fault 2. This cycle will repeat into the future as the faults toggle back and forth as they trade off slip to maintain a steady system-level rate.

Table 1 Summary of age and displacement data and incremental fault slip rates for the four main Marlborough system faults. The first column shows the age range over which each incremental slip rate is averaged in kilo-years before present (ka). The second column shows the duration of that increment. The third column shows the displacement ranges over which that incremental rate was averaged, and the fourth column shows the displacement that occurred during that increment. The fifth column shows the resulting incremental slip rate for that increment, as discussed in this paper, and summarized in figures 3, 4, and 5. The sixth column shows the percentage overlap between the probability density functions of that incremental rate relative to the preceding incremental rate, using the methodology of (Pastore & Calcagni, 2019). These values demonstrate the variability of the incremental rates through on each of the Marlborough faults. See Supplemental text for details of our statistical analysis. Time and displacement measurements are reported with 95% confidence limits. Slip rate values are reported with 68% confidence limits.

References

Ashby, M.F., and Verrall, R.A., 1978, Micromechanisms of Flow and Fracture, and their Relevance to the Rheology of the Upper Mantle: *Philosophical Transactions of the Royal Society of London. Series A, Mathematical and Physical Sciences*, v. 288, (1350), Creep of Engineering Materials and of the Earth (Feb. 14, 1978), p. 59-93.

Bak. P., Tang, C., 1989, Earthquakes as a self-organized critical phenomenon: *Journal of Geophysical Research*, v. 94, B11, p. 15635-15637, https://doi.org/10.1029/JB094iB11p15635

Beavan, J., Tregoning, P., Bevis, M., Kato, T. & Meertens, C., 2002, Motion and rigidity of the Pacific Plate and implications for plate boundary deformation: *Journal of Geophysical Research*, v. 107(B10), doi: 10.1029/2001JB000282.

Berryman, K. R., Cochran, U. A., Clark, K. J., Biasi, G. P., Langridge, R. M., and Villamor, P., 2012, Major earthquakes occur regularly on an isolated Plate Boundary Fault: *Science*, v. 336, p. 1690–1693, https://doi.org/10.1126/science.1218959

Bufe, C.G., Harsh, P.W., and Burford, R.O., 1977, Steady-state seismic slip – A precise recurrence model: *Geophysical Research Letters*, v. 4 (2), p. 91-94, https://doi.org/10.1029/GL004i002p00091

Bürgmann, R., and Dresen, G., 2008, Rheology of the lower crust and upper mantle: Evidence from rock mechanics, geodesy, and field observations: *Annual Reviews of Earth and Planetary Sciences*, v. 36, p. 531–567, 10.1146/annurev.earth.36.031207.124326

Chen, Y., Liu, M., and Luo, G., 2020, Complex temporal patterns of large earthquakes: Devil's staircases: Bulletin of the Seismological Society of America, v. 110(3), p. 1064–1076, https://doi.org/10.1785/0120190148

Dawson, T. E., S. F. McGill, and T. K. Rockwell (2003), Irregular recurrence of paleoearthquakes along the central Garlock fault near El Paso Peaks, California: *Journal of Geophysical Research, Solid Earth*, v. 108(B7), doi:10.1029/2001JB001744.

DeMets, C., Gordon, R. G., Argus, D. F., and Stein, S., 1990, Current plate motions: *Geophysical Journal International, v. 101, p. 425-478.*

DeMets, C., Gordon, R. G., Argus, D. F., and Stein, S., 1994, Effect of recent revisions to the geomagnetic reversal time scale on estimates of current plate motions: *Geophysical Research Letters*, v. 21(20), p. 2191–2194, https://doi.org/10.1029/94gl02118

DeMets, C., Gordon, R.G., and Argus, D.F., 2010, Geologically current plate motions: *Geophysical Journal International*, v. 181, p. 1–80, https:// doi .org /10 .1111 /j .1365 -246X .2009 .04491 .x.

Dolan, J. F., and Haravitch, B. D., 2014, How well do surface slip measurements track slip at depth in large strike-slip earthquakes? The importance of structural maturity in controlling on-fault versus off-fault deformation: *Earth and Planetary Science Letters*, http://dx.doi.org/10.1016/j.epsl.2013.11.043.

Dolan, J. F., Bowman, D. D., and Sammis, C. G., 2007, Long-range and long-term fault interactions in Southern California: *Geology*, v. 35(9), p. 855–858, https://doi.org/10.1130/g23789a.1

Dolan, J. F., Bowman, D. D., and Sammis, C. G., 2007, Long-range and long-term fault interactions in southern California: *Geology*, v. 35, p. 855-858.

Dolan, J. F., McAuliffe, L. J., Rhodes, E. J., McGill, S., & Zinke, R. W., 2016, Extreme multi-millennial slip rate variations on the Garlock fault, California: Strain super-cycles, potentially time-variable fault strength, and implications for system-level earthquake occurrence: *Earth and Planetary Science Letters*, v. 446, p. 123–136, https://doi.org/10.1016/j.epsl.2016.04.011

Dolan, J. F., and Meade, B. J., 2017, A comparison of geodetic and geologic rates prior to large strike-slip earthquakes: A diversity of earthquake-cycle behaviors? *Geochemistry, Geophysics, Geosystems*, v. 18(12), p. 4426–4436, https://doi.org/10.1002/2017GC007014

Eberhart-Phillips, D., and Bannister, S., 2010, 3-D imaging of Marlborough, New Zealand, subducted plate and strike-slip fault systems: *Geophysical Journal International*, v. 182, p. 73-96, doi: 10.1111/j.1365-246X.2010.04621.x

Eberhart-Phillips, D., M. Reyners, S. Bannister, M. Chadwick, and S. Ellis, S., 2010, Establishing a versatile 3D seismic velocity model for New Zealand: *Seismological Research Letters*, v. 81, no. 6, p. 992–1000, doi: 10.1785/gssrl.81.6.992.

Eberhart-Phillips, D., Bannister, S., and Ellis, S., 2014, Imaging *P* and *S* attenuation in the termination region of the Hikurangi subduction zone, New Zealand: *Geophysical Journal International*, v. 198, p. 516-536, doi: 10.1093/gji/ggu151.

Evans, E.L., 2018, A Comprehensive Analysis of Geodetic Slip-Rate Estimates and Uncertainties in California: *Bulletin of the Seismological Society of America*, v. 108, No. 1, p. 1–18, February 2018, doi: 10.1785/0120170159

Fay, N. and Humphreys, E., 2006, Dynamics of the Salton block: Absolute fault strength and crust-mantle coupling in Southern California: *Geology*, v. 34; no. 4; p. 261–264; doi: 10.1130/G22172.1

Fialko, Y., Rivera, L., and Kanamori, H., 2004, Estimate of differential stress in the upper crust from variations in topography and strike along the San Andreas fault: *Geophysical Journal International*, v. 160, p. 527-532, doi: 10.1111/j.1365-246X.2004.02511.x

Fialko, Y., 2021, Estimation of Absolute Stress in the Hypocentral Region of the 2019 Ridgecrest, California, Earthquakes: *Journal of Geophysical Research*, 10.1029/2021JB022000

Field, E. H., Biasi, G. P., Bird, P., Dawson, T. E., Felzer, K. R., Jackson, D. D., et al., 2015, Long-term time-dependent probabilities for the third Uniform California Earthquake Rupture Forecast (UCERF3): *Bulletin of the Seismological Society of America*, v. 105(2A), p. 511–543, https://doi.org/10.1785/0120140093

Field, E.H., Jordan, T.H., Jones, L.M., Michael, A.J., Blanpied, M.L., et al., 2016, The potential uses of Operational Earthquake Forecasting: *Seismological Research Letters*, v. 87 (2A), p. 313–322, https://doi.org/10.1785/0220150174

Field, E. H., Jordan, T. H., Page, M. T., Milner, K. R., Shaw, B. E., Dawson, T. E., et al., 2017, A Synoptic view of the third Uniform California Earthquake Rupture Forecast (UCERF3): *Seismological Research Letters*, v. 88(5), p. 1259–1267, https://doi.org/10.1785/0220170045

Field, E. H., 2019, How physics-based earthquake simulators might help improve earthquake forecasts: *Seismological Research Letters*, v. 90, p. 467-472, doi:https://doi.org/10.1785/0220180299

Finch, M.A., Weinberg, R.F., and Hunter, N.J.R., 2016, Water loss and the origin of thick ultramylonites: *Geology*, v. 44, p. 599-602, doi:10.1130/G37972.1

Friedrich, A. M., Wernicke, B. P., Niemi, N. A., Bennett, R. A., & Davis, J. L., 2003, Comparison of geodetic and geologic data from the Wasatch region, Utah, and implications for the spectral character of Earth deformation at periods of 10 to 10 million years: *Journal of Geophysical Research*, v. 108(B4), https://doi.org/10.1029/2001JB000682

Gauriau, J., and Dolan, J.F., 2021, Relative structural complexity of plate-boundary fault systems controls incremental slip-rate behavior of major strike-slip faults: *Geochemistry, Geophysics, Geosystems*, v. 22 (11), e2021GC009938, https://doi.org/10.1029/2021GC009938.

Gauriau, J., Barbot, S., and Dolan, J.F., 2023, Islands of chaos in a sea of periodic earthquakes: *Earth and Planetary Science Letters*, 618, 118274, https://doi.org/10.1016/j.epsl.2023.118274.

Gold, R. D., and Cowgill, E., 2011, Deriving fault-slip histories to test for secular variation in slip, with examples from the Kunlun and Awatere faults: *Earth and Planetary Science Letters*, v. 301(1), p. 52–64, https://doi.org/10.1016/j.epsl.2010.10.011

Harris, R.A., 1998, Introduction to Special Section: Stress Triggers, Stress Shadows, and Implications for Seismic Hazard: *Journal of Geophysical Research*, https://doi.org/10.1029/98JB01576

Harris, R. A., & Simpson, R. W., 1996, In the shadow of 1857 - the effect of the Great Fort Tejon Earthquake on subsequent earthquakes in southern California: *Geophysical Research Letters*, v. 23(3), p. 229–232, https://doi.org/10.1029/96GL00015

Harris, R.A., and Simpson, R.W., 1998, Suppression of large earthquakes by stress shadows: A comparison of Coulomb and rate-and-state failure: *Journal of Geophysical Research*, v. 103, p. 24,439-24,451.

Hartleb, R. D., Dolan, J. F., and Kozacı, Ö., 2006, A 2500-yr-long paleoseismologic record of large, infrequent earthquakes on the North Anatolian fault at Çukurçimen, Turkey: *Geological Society of America Bulletin*, v. 118(7–8), p. 823–840, https://doi.org/10.1130/b25838.1

Hatem, A.E., Dolan, J.F., Zinke, R.W., Langridge, R.M., McGuire, C.M., Rhodes, E.J., Brown, N., Van Dissen, R.J., 2020, Holocene to latest Pleistocene incremental slip rates from the east-central Hope fault (Conway segment) at Hossack Station, Marlborough fault system, South Island, New Zealand: Towards a dated path of earthquake slip along a plate boundary fault: *Geosphere*, v. 16 (6), p. 1558-1584, https://doi.org/10.1130/GES02263.1

Jordan, T. H., Marzocchi, W., Michael, A. J., and Gerstenberger, M. C., 2014, Operational earthquake forecasting can enhance earthquake preparedness: *Seismological Research Letters*, v. 85, p. 955-959, https://doi.org/10.1785/0220140143.

Kondo, H., Özaksoy, V., Yıldirim, C., Awata, Y., Emre, Ö., & Okumura, K., 2004, 3D trenching survey at Demir Tepe site on the 1944 earthquake rupture, North Anatolian fault system, Turkey: *Seismological Research Letters, v. 75(2).*

Kozacı, Ö., Dolan, J. F., Finkel, R. C., and Hartleb, R. D., 2007, A 2000-year slip rate for the North Anatolian fault, Turkey, from cosmogenic ^{36}Cl geochronology: Implications for the constancy of fault loading and slip rates: *Geology*, v. 35, p. 867-870; doi:10.1130/G23187A.1.

Kozacı, Ö., Dolan, J.F., and Finkel, R.C., 2009, Late Holocene slip rate for the central North Anatolian fault, Tahtakorpru, Turkey, from Cosmogenic ^{10}Be Geochronology: Implications for the constancy of fault loading and strain release rates: *Jour. Geophys. Res*., 114, doi:10.1029/2008JB005760, 2009.

Kronenberg, A.K., Ashley, K.T., Francsis, M.K., Holyoke, C.W., III, Jezek, L., Kronenberg, J.A., Law, R.D., and Thomas, J.B., 2020, Water loss during dynamic recrystallization of Moine thrust quartzites, northwest Scotland: Geology, v. 48. P. 557-561, https://doi.org/10.1130/G47041.1

Lensen, G. J., 1968, Analysis of progressive fault displacement during downcutting at the Branch River terraces, South Island, New Zealand: *Geological Society of America Bulletin*, v. 79, p. 545–556. https://doi.org/10.1130/0016 7606(1968)79[545:aopfdd]2.0.co;2

Nicol, A., and Van Dissen, R., 2018, A 6000-year record of surface-rupturing paleoearthquakes on the Wairau Fault, New Zealand: *New Zealand Journal of Geology and Geophysics*, https://doi.org/10.1080/00288306.2018.1498360.

Ninis, D., Little, T. A., Dissen, R. J. V., Litchfield, N. J., Smith, E. G. C., Wang, N., et al., 2013, Slip rate on the Wellington Fault, New Zealand, during the Late Quaternary: Evidence for Variable Slip during the Holocene: *Bulletin of the Seismological Society of America*, v. 103(1), p. 559–579. https://doi.org/10.1785/0120120162

Noriega, G. R., Arrowsmith, J. R., Grant, L. B., & Young, J. J., 2006, Stream Channel Offset and Late Holocene Slip Rate of the San Andreas fault at the Van Matre Ranch Site, Carrizo Plain, California: *Bulletin of the Seismological Society of America*, v. 96(1), p. 33–47. https://doi.org/10.1785/0120050094

Oskin, M., L. Perg, E. Shelef, M. Strane, E. Gurney, B. Singer, and X. Zhang, 2008, Elevated shear zone loading rate during an earthquake cluster in eastern California: *Geology*, v. 36(6), p. 507–510, doi:10.1130/G24814A.1.

Pastore, M., and Calcagni, A., 2019, Measuring Distribution Similarities Between Samples: A Distribution-Free Overlapping Index: *Frontiers in Psychology*, v. 10, article 1089, *doi: 10.3389/fpsyg.2019.01089.*

Peña, K., McGill, S., Rhodes, E.J., Dolan, J.F., Zinke, R., Hatem, A., and Brown, N., 2018, Paleoseismology of the central Garlock fault in Searles Valley, California: *Geological Society of America, Proceedings of GSA Annual Meeting* (abstract), DOI:10.1130/abs/2018AM-321087.

Pucci, S., De Martini, P. M., & Pantosti, D., 2008, Preliminary slip rate estimates for the Düzce segment of the North Anatolian Fault Zone from offset geomorphic markers: *Geomorphology*, v. 97(3), p. 538–554, https://doi.org/10.1016/j.geomorph.2007.09.002

Rattenbury, M.S., Townsend, D.B., and Johnston, M.R. (compilers), 2006, Geology of the Kaikoura area: *New Zealand Institute of Geological & Nuclear Sciences* 1:250 000 Geological Map 13, scale 1:250,000, 1 sheet, 70 p. text.

Rhodes, E.J., 2015, Dating sediments using potassium feldspar single-grain IRSL: Initialmethodological considerations: *Quaternary International*, v.362, p.14-22, https://doi.org/10.1016/j.quaint.2014.12.012

Salisbury, J. B., Arrowsmith, J. R., Brown, N. D., Rockwell, T., Sinan, A., and Grant Ludwig, L. B., 2018, The age and origin of small offsets at Van Matre Ranch along the San Andreas Fault in the Carrizo Plain, California: *Bulletin of the Seismological Society of America*, v. 108(2), p. 639–653. https://doi.org/10.1785/0120170162

Seebeck, H., Van Dissen, R., Litchfield, N., Barnes, P.M., Nicol, A., Langridge, R., Barrell, J.A., Villamor, P., et al. 2023, The New Zealand Community Fault Model – version 1.0: an improved geological foundation for seismic hazard modelling: *New Zeland Journal of Geology and Geophysics*, https://doi.org/10.1080/00288306.2023.2181362

Shimazaki. K., and Nakata, T.,1980, Time-predictable recurrence model for large earthquakes: *Geophysical Research Letters*, v. 7 (4), p. 279-282, https://doi.org/10.1029/GL007i004p00279.

Sutherland, R., 1999, Basement geology and tectonic development of the greater New Zealand region: An interpretation from regional magnetic data: *Tectonophysics*, v. 308(3), p. 341–362. https://doi.org/10.1016/S0040-1951(99)00108-0

Van Dissen, R., Abbott, E., Zinke, R., Ninis, D., Dolan, J., Little, T., Rhodes, E., Litchfield, N., Hatem, A., 2020, Slip rate variations on major strike-slip faults in central New Zealand and potential impacts on hazard estimation: *Proceedings of the 2020 New Zealand Society for Earthquake Engineering Annual Technical Conference*, https://repo.nzsee.org.nz/handle/nzsee/1691.

Wallace, L. M., Beavan, J., McCaffrey, R., Berryman, K., and Denys, P., 2007, Balancing the plate motion budget in the South Island, New Zealand using GPS, geological and seismological data: *Geophysical Journal International*, v. 168, p. 332–352.

Wallace, R. E., 1987, Grouping and migration of surface faulting and variations in slip rates on faults in the Great Basin province: *Bulletin of the Seismological Society of America*, v. 77(3), p. 868–876.

Weldon, R., Scharer, K., Fumal, T., and Biasi, G., 2004, Wrightwood and the earthquake cycle: What a long recurrence record tells us about how faults work: *Geological Society of America Today*, v. 14(9), p. 4–10, https://doi.org/10.1130/1052-5173(2004)014<4:watecw>2.0.co;2

Williams, C.A., Eberhart-Phillips, D., Bannister, S., Barker, D.H.N., Henrys, S. Reyners, M., and Sutherland, R., 2013, Revised Interface Geometry for the Hikurangi Subduction Zone, New Zealand: *Seismological Research Letters*, v. 84, 6, doi: 10.1785/0220130035

Zinke, R., Dolan, J. F., Van Dissen, R., Grenader, J. R., Rhodes, E. J., McGuire, C.P., Langridge, R., Nicol, A., and Hatem, A., 2015, Progressive geomorphic and structural manifestation of fault slip as a function of cumulative displacement: A comparison of the Wairau and Awatere faults, South Island, New Zealand: *Geology*, doi:10.1130/G37065.1, Data Repository item 2015341.

Zinke, R., Dolan, J.F., Rhodes, E.J., Van Dissen, R., and McGuire, C.P., 2017, Highly variable latest Pleistocene–Holocene incremental slip rates on the Awatere fault at Saxton River, South Island, New Zealand, revealed by lidar mapping and luminescence dating: *Geophysical Research Letters*, v. 44, doi:10.1002/2017GL075048.

Zinke, R. W., Dolan, J. F., Rhodes, E.J., Van Dissen, R.J., McGuire, C.P., Hatem, A.E., and Brown, N.D., 2019, Multimillennial incremental slip rate variability of the Clarence fault at the Tophouse Road site, Marlborough fault system, New Zealand: *Geophysical Research Letters*, v. 46 (2), p. 717-725, https://doi.org/10.1029/2018GL080688.

Zinke, R., Dolan, J.F., Rhodes, E.J., Van Dissen, R.J., Hatem, A.E., McGuire, C.P., Brown, N.A., Grenader, J.R., 2021, Latest Pleistocene–Holocene Incremental Slip Rates of the Wairau Fault: Implications for Long-Distance and Long-Term Coordination of Faulting Between North and South Island, New Zealand: *Geochemistry, Geophysics, Geosystems*, v. 22 (9), e2021GC009656, https://doi.org/10.1029/2021GC009656.

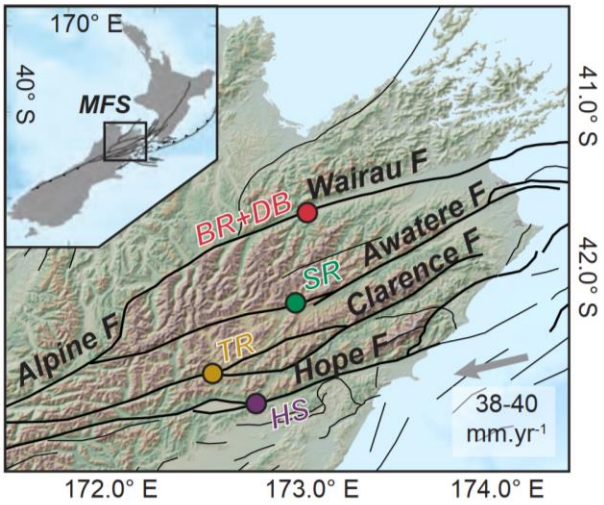

Figure 1.

Figure 2.

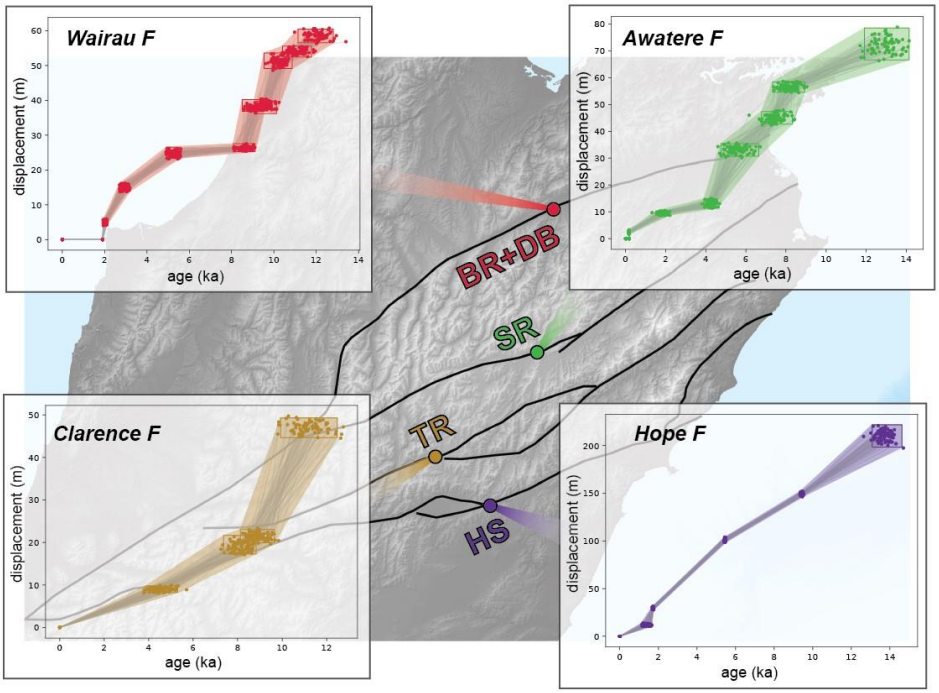

Figure 3.

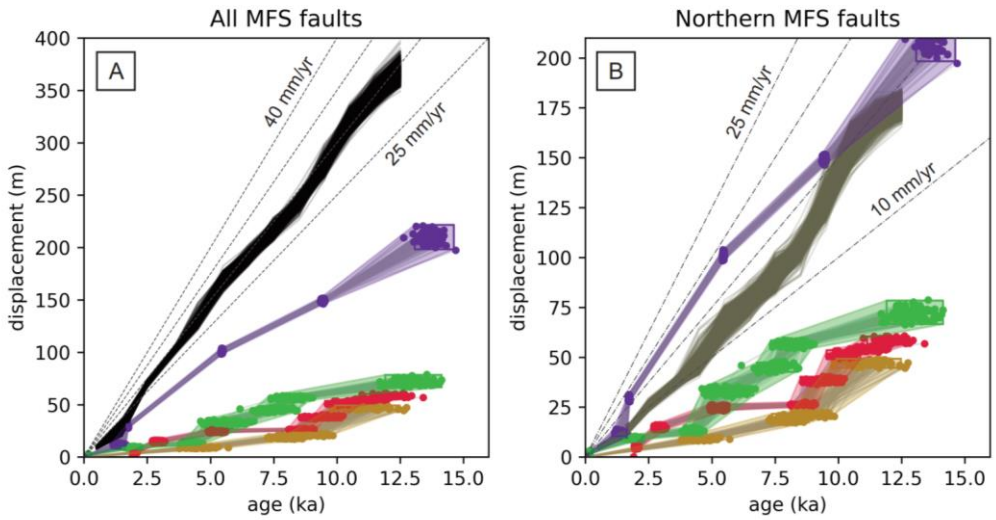

Figure 4.

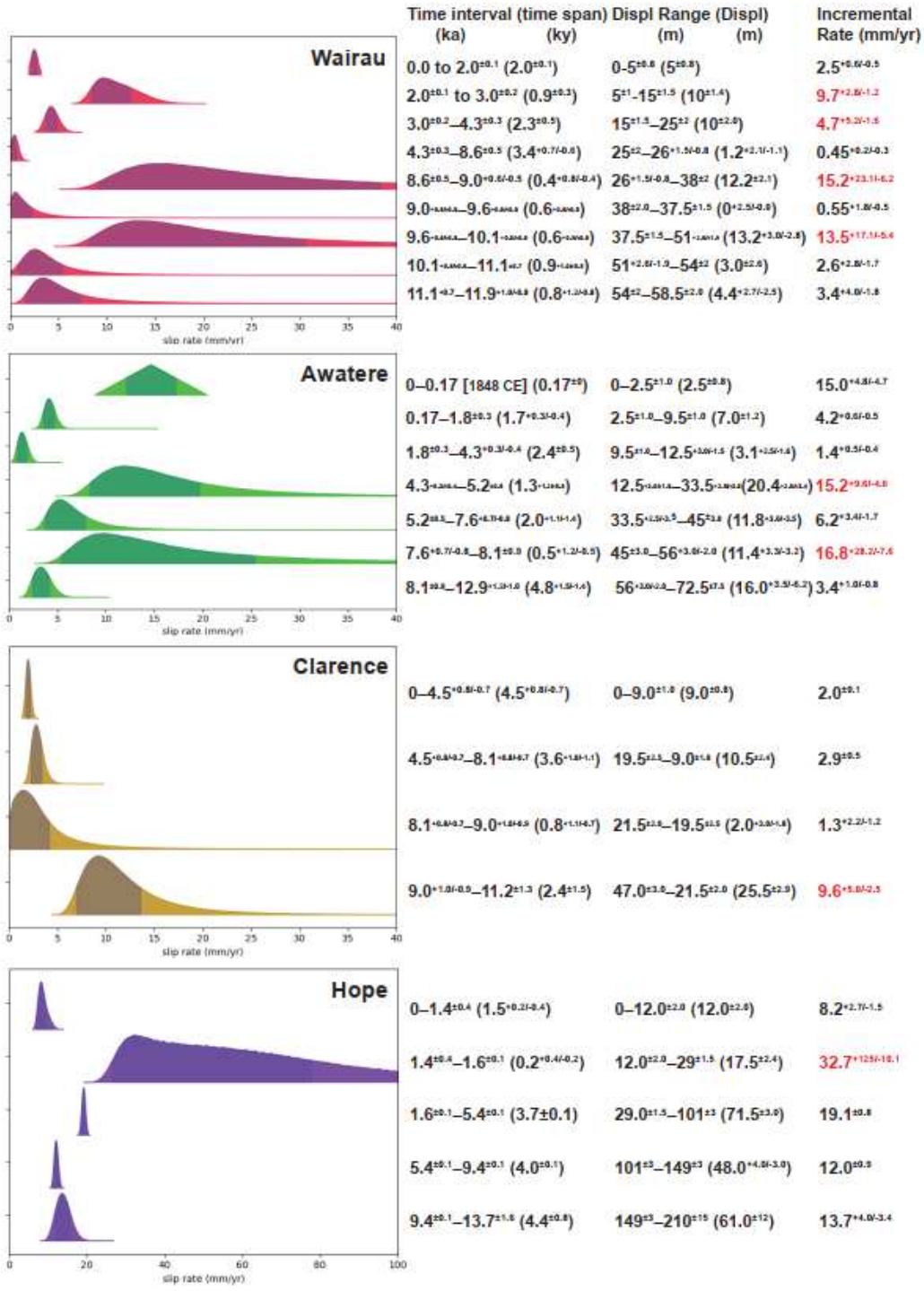
Time interval (time span) (ka) (ky)
Displ Range (Displ) (m) (m)
Incremental Rate (mm/yr)
Wairau
0.0 to 2.0±0.1 (2.0±0.1) 0-5±0.8 (5±0.8) 2.5+0.6/-0.5
2.0±0.1 to 3.0±0.2 (0.9±0.3) 5±1-15±1.5 (10±1.4) 9.7+2.8/-1.2
3.0±0.2–4.3±0.3 (2.3±0.5) 15±1.5–25±2 (10±2.0) 4.7+5.2/-1.5
4.3±0.3–8.6±0.5 (3.4+0.7/-0.6) 25±2–26+1.5/-0.8 (1.2+2.1/-1.1) 0.45+0.2/-0.3
8.6±0.5–9.0+0.6/-0.5 (0.4+0.8/-0.4) 26+1.5/-0.8–38±2 (12.2±2.1) 15.2+23.1/-6.2
9.0–9.6 (0.6) 38±2.0–37.5±1.5 (0+2.5/-0.8) 0.55+1.8/-0.5
9.6–10.1 (0.6) 37.5±1.5–51 (13.2+3.0/-2.8) 13.5+17.1/-5.4
10.1–11.1±0.7 (0.9) 51+2.6/-1.9–54±2 (3.0±2.6) 2.6+2.8/-1.7
11.1±0.7–11.9+1.8/-1.8 (0.8+1.2/-0.8) 54±2–58.5±2.0 (4.4+2.7/-2.5) 3.4+4.8/-1.8
slip rate (mm/yr)
Awatere
0–0.17 [1848 CE] (0.17±0) 0–2.5±1.0 (2.5±0.8) 15.0+4.8/-4.7
0.17–1.8±0.3 (1.7+0.3/-0.4) 2.5±1.0–9.5±1.0 (7.0±1.2) 4.2+0.6/-0.5
1.8±0.3–4.3+0.3/-0.4 (2.4±0.5) 9.5±1.0–12.5+3.0/-1.5 (3.1+2.5/-1.4) 1.4+0.5/-0.4
4.3–5.2±0.4 (1.3) 12.5–33.5 (20.4) 15.2+9.6/-4.8
5.2±0.5–7.6+0.7/-0.8 (2.0+1.1/-1.4) 33.5+2.5/-3.5–45±3.8 (11.8+3.6/-3.5) 6.2+3.4/-1.7
7.6+0.7/-0.8–8.1±0.9 (0.5+1.2/-0.5) 45±3.0–56+3.6/-2.0 (11.4+3.3/-3.2) 16.8+28.2/-7.6
8.1±0.8–12.9+1.3/-1.0 (4.8+1.9/-1.4) 56+3.6/-2.0–72.5±7.5 (16.0+3.5/-6.2) 3.4+1.6/-0.8
slip rate (mm/yr)
Clarence
0–4.5+0.8/-0.7 (4.5+0.8/-0.7) 0–9.0±1.0 (9.0±0.8) 2.0±0.1
4.5+0.8/-0.7–8.1+0.8/-0.7 (3.6+1.6/-1.1) 19.5±2.5–9.0±1.0 (10.5±2.4) 2.9±0.5
8.1+0.8/-0.7–9.0+1.6/-0.9 (0.8+1.1/-0.7) 21.5±2.5–19.5±2.5 (2.0+3.6/-1.4) 1.3+2.2/-1.2
9.0+1.6/-0.9–11.2±1.3 (2.4±1.5) 47.0±3.0–21.5±2.0 (25.5±2.9) 9.6+5.6/-2.3
slip rate (mm/yr)
Hope
0–1.4±0.4 (1.5+0.2/-0.4) 0–12.0±2.0 (12.0±2.8) 8.2+2.7/-1.5
1.4±0.4–1.6±0.1 (0.2+0.4/-0.2) 12.0±2.0–29±1.5 (17.5±2.4) 32.7+125/-18.1
1.6±0.1–5.4±0.1 (3.7±0.1) 29.0±1.5–101±3 (71.5±3.0) 19.1±0.8
5.4±0.1–9.4±0.1 (4.0±0.1) 101±3–149±3 (48.0+4.6/-3.0) 12.0±0.9
9.4±0.1–13.7±1.6 (4.4±0.8) 149±3–210±15 (61.0±12) 13.7+4.6/-3.4
slip rate (mm/yr)

Figure 5.

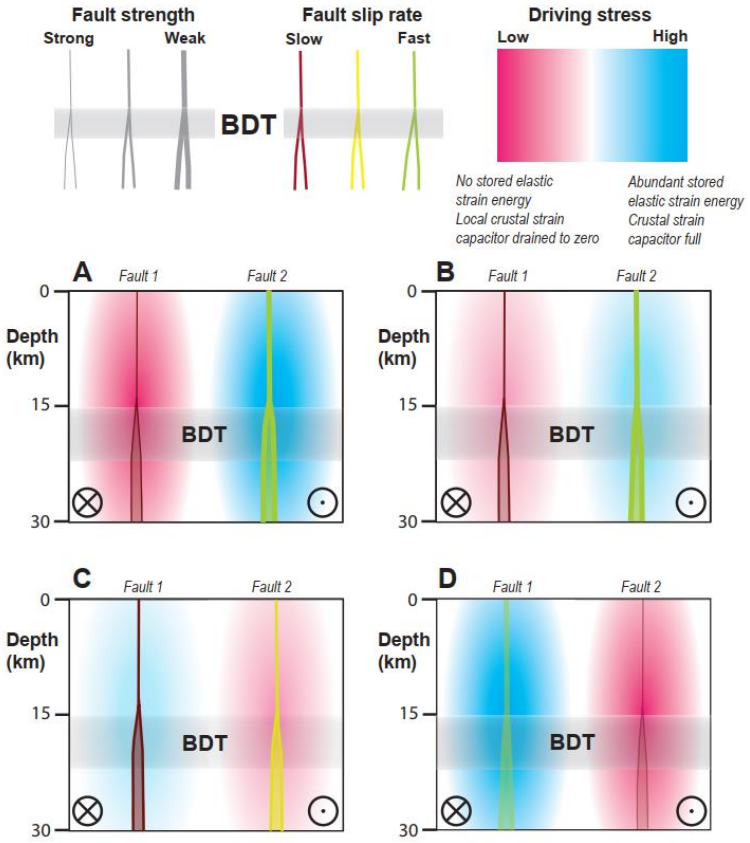
Fault strength
Strong
Weak
BDT
Fault slip rate
Slow
Fast
Driving stress
Low
High
No stored elastic strain energy
Local crustal strain capacitor drained to zero
Abundant stored elastic strain energy
Crustal strain capacitor full
A
B
C
D
Fault 1
Fault 2
Depth (km)
0
15
30
BDT

Figure 6.

Wairau fault

Time interval (ka)	Time span (ky)	Cumulative disp (m)	Disp interval (m)	Slip rate (mm/yr)	PDF overlap
0.0 to $2.0^{\pm0.1}$	$2.0^{\pm0.1}$	0 to $5^{\pm1}$**	$5^{\pm0.8}$	$2.5^{+0.6/-0.5}$	
$2.0^{\pm0.1}$ to $3.0^{\pm0.2}$	$0.9^{\pm0.3}$	$5^{\pm1}$ to $15^{\pm1.5}$	$10^{\pm1.4}$	$9.7^{+2.8/-1.2}$	0.00
$3.0^{\pm0.2}$ to $4.3^{\pm0.3}$	$2.3^{\pm0.5}$	$15^{\pm1.5}$ to $25^{\pm2}$	$10^{\pm2.0}$	$4.7^{+5.2/-1.6}$	0.00
$4.3^{\pm0.3}$ to $8.6^{\pm0.5}$	$3.4^{+0.7/-0.6}$	$25^{\pm2}$ to $26^{+1.5/-0.8}$	$1.2^{+2.1/-1.1}$	$0.45^{+0.2/-0.3}$*	0.00
$8.6^{\pm0.5}$ to $9.0^{+0.6/-0.5}$	$0.4^{+0.8/-0.4}$	$26^{+1.5/-0.8}$ to $38^{\pm2}$	$12.2^{\pm2.1}$	$15.2^{+23.1/-6.2}$	0.00
$9.0^{+0.6/-0.5}$ to $9.6^{+0.6/-0.5}$	$0.6^{+0.8/-0.5}$	$38^{\pm2.0}$ to $37.5^{\pm1.5}$	$0^{+2.5/-0.0}$	$0.55^{+1.8/-0.5}$*	0.07
$9.6^{+0.6/-0.5}$ to $10.1^{+0.8/-0.6}$	$0.6^{+0.9/-0.5}$	$37.5^{\pm1.5}$ to $51^{+2.6/-1.9}$	$13.2^{+3.0/-2.8}$	$13.5^{+17.1/-5.4}$	0.08
$10.1^{+0.8/-0.6}$ to $11.1^{+0.7}$	$0.9^{+1.0/-0.8}$	$51^{+2.6/-1.9}$ m to $54^{\pm2}$	$3.0^{\pm2.6}$	$2.6^{+2.8/-1.7}$	0.15
$11.1^{+0.7}$ to $11.9^{+1.0/-0.8}$	$0.8^{+1.2/-0.8}$	$54^{\pm2}$ to $58.5^{\pm2.0}$	$4.4^{+2.7/-2.5}$	$3.4^{+4.0/-1.8}$	0.79

*slip rate likely 0 mm/yr during these intervals; **Smallest slip increment ($5^{\pm1}$ m) is assumed to have occurred during ca. 2.0 ka most recent earthquake (Nicol et al., 2011; Nicol & Van Dissen, 2018; Zinke et al., 2021)

Awatere fault

Time interval (ka)	Time span (ky)	Cumulative disp (m)	Disp interval (m)	Slip rate (mm/yr)	PDF overlap
0 to 0.17*	$0.17^{\pm0}$	0 to $2.5^{\pm1.0}$	$2.5^{\pm0.8}$	$15.0^{+4.8/-4.7}$	
0.17* to $1.8^{\pm0.3}$	$1.7^{+0.3/-0.4}$	$2.5^{\pm1.0}$ to $9.5^{\pm1.0}$	$7.0^{\pm1.2}$	$4.2^{+0.6/-0.5}$	0.00
$1.8^{\pm0.3}$ to $4.3^{+0.3/-0.4}$	$2.4^{\pm0.5}$	$9.5^{\pm1.0}$ to $12.5^{+3.0/-1.5}$	$3.1^{+2.5/-1.6}$	$1.4^{+0.5/-0.4}$	0.01
$4.3^{+0.3/-0.4}$ to $5.2^{\pm0.5}$	$1.3^{+1.2/-0.8}$	$12.5^{+3.0/-1.5}$ to $33.5^{+2.5/-3.5}$	$20.4^{+2.8/-3.4}$	$15.2^{+9.6/-4.6}$	0.00
$5.2^{\pm0.5}$ to $7.6^{+0.7/-0.8}$	$2.0^{+1.1/-1.4}$	$33.5^{+2.5/-3.5}$ to $45^{\pm3.0}$	$11.8^{+3.6/-3.5}$	$6.2^{+3.4/-1.7}$	0.25
$7.6^{+0.7/-0.8}$ to $8.1^{\pm0.9}$	$0.5^{+1.2/-0.5}$	$45^{\pm3.0}$ to $56^{+3.0/-2.0}$	$11.4^{+3.3/-3.2}$	$16.8^{+28.2/-7.6}$	0.34
$8.1^{\pm0.9}$ to $12.9^{+1.2/-1.0}$	$4.8^{+1.5/-1.4}$	$56^{+3.0/-2.0}$ to $72.5^{\pm7.5}$	$16.0^{+3.5/-6.2}$	$3.4^{+1.0/-0.8}$	0.03

* ~2.5 m of displacement occurred at this site during the 1848 Canterbury earthquake (Mason et al., 2004; Zinke et al., 2017)

Clarence fault

Time interval (ka)	Time span (ky)	Cumulative disp (m)	Disp interval (m)	Slip rate (mm/yr)	PDF overlap
0 to $4.5^{+0.8/-0.7}$	$4.5^{+0.8/-0.7}$	0 to $9.0^{\pm1.0}$	$9.0^{\pm0.8}$	$2.0^{\pm0.1}$	
$4.5^{+0.8/-0.7}$ to $8.1^{+0.8/-0.7}$	$3.6^{+1.0/-1.1}$	$19.5^{\pm2.5}$ to $9.0^{\pm1.0}$	$10.5^{\pm2.4}$	$2.9^{\pm0.5}$	0.23
$8.1^{+0.8/-0.7}$ to $9.0^{+1.0/-0.9}$	$0.8^{+1.1/-0.7}$	$21.5^{\pm2.0}$ to $19.5^{\pm2.5}$	$2.0^{+3.0/-1.8}$	$1.3^{+2.2/-1.2}$**	0.40
$9.0^{+1.0/-0.9}$ to $11.2^{\pm1.3}$	$2.4^{\pm1.5}$	$47.0^{\pm3.0}$ to $21.5^{\pm2.0}$	$25.5^{\pm2.9}$	$9.6^{+5.0/-2.5}$	0.19

* displacement possibly 0 mm during this interval; **slip rate possibly 0 mm/yr during this interval

Hope fault

Time interval (ka)	Time span (ky)	Cumulative disp (m)	Disp interval (m)	Slip rate (mm/yr)	PDF overlap
0.0 to $1.4^{\pm0.4}$	$1.5^{+0.2/-0.4}$	0 to $12.0^{\pm2.0}$	$12.0^{\pm2.0}$	$8.2^{+2.7/-1.5}$	
$1.4^{\pm0.4}$ to $1.6^{\pm0.1}$	$0.2^{+0.4/-0.2}$	$12.0^{\pm2.0}$ to $29^{\pm1.5}$	$17.5^{\pm2.4}$	$32.7^{+125/-10.1}$	0.00
$1.6^{\pm0.1}$ to $5.4^{\pm0.1}$	$3.7^{\pm0.1}$	$29.0^{\pm1.5}$ to $101^{\pm3}$	$71.5^{\pm3.0}$	$19.1^{\pm0.8}$	0.00
$5.4^{\pm0.1}$ to $9.4^{\pm0.1}$	$4.0^{\pm0.1}$	$101^{\pm3}$ to $149^{\pm3}$	$48.0^{+4.0/-3.0}$	$12.0^{\pm0.9}$	0.00
$9.4^{\pm0.1}$ to $13.7^{\pm1.6}$	$4.4^{\pm0.8}$	$149^{\pm3}$ to $210^{\pm15}$	$61.0^{\pm12}$	$13.7^{+4.0/-3.4}$	0.34